Composites Part B 278 (2024) 111410

Contents lists available at ScienceDirect

Composites Part B

journal homepage: www.elsevier.com/locate/compositesb

ECM-based Ca^{2+}/L-arginine/NO periosteum nourishes bone defect microenvironment, directs macrophage polarity, and accelerates osteogenesis and angiogenesis

Ho-Pan Bei [a,b,c], Xiongfa Ji [b,c,d], Tianpeng Xu [a,b,c], Zhenhua Chen [b,c], Chun-Hei Lam [b], Xintong Zhou [a,c], Yuhe Yang [a,b,c], Yu Zhang [d], Chunyi Wen [b], Yaxiong Liu [e,f], Xin Zhao [a,b,c,*]

[a] Department of Applied Biology and Chemical Technology, the Hong Kong Polytechnic University, Hung Hom, Kowloon, China
[b] Department of Biomedical Engineering, the Hong Kong Polytechnic University, Hung Hom, Kowloon, China
[c] The Hong Kong Polytechnic University Shenzhen Research Institute, Shenzhen, China
[d] Department of Orthopedics, Guangdong Provincial People's Hospital, Guangdong Academy of Medical Sciences, Southern Medical University, China
[e] School of Mechatronic Engineering and Automation, Foshan University, Foshan, China
[f] Ji Hua Laboratory, Foshan, China

ARTICLE INFO

Handling Editor: Dr Hao Wang

Keywords:
A. Fibres
A. Nano-structures
A. Polymer-matrix composites
E. Electrospinning (nominated)

ABSTRACT

The natural periosteum is responsible for supporting bone homeostasis and initiating repair, but is often damaged during bone fracture, causing acute inflammation and loss of a functioning substratum for induction of new bone formation. Here, we propose an ECM-based Ca^{2+}/L-arginine/nitric oxide (NO) electrospun periosteum to reinitiate bone regeneration. The multifaceted action of NO could promote osteoblastic differentiation, angiogenesis and polarization of macrophages, while accelerating new bone formation, enhancing bone quality and reducing inflammation in a rat critical size calvarial defect model, acting as a mainspring that drives the rest of the PI3K-AKT pathway including the downstream action of VEGF, MAPK and mTOR signalling. The modulation of NO cycle by periosteum scaffold is envisioned to be highly efficient at supporting bone grafting surgeries, with simple and clean clinical translation and implications for anti-inflammatory healing.

1. Introduction

The term "scaffold" is originally coined to describe a temporary framework for the construction, maintenance and repair of building structures [1]. As tissue engineering scaffolds evolve, generations of biomaterials are fabricated to aid in the regeneration of injuries, replacement of broken tissues and even integration into the host by bio-resorption; the adaptability to complex microstructures and ability to serve diverse functions far eclipsing their progenitors to match the natural ambience of living organisms [2,3]. The periosteum is one such scaffold: a tight, fibrous membrane of collagen fibers capable of supporting bone homeostasis through its abundantly housed osteoblasts, mesenchymal stem cells (MSCs), capillaries and macrophages [4,5]. Its nourishment and reservoir of pluripotent MSCs and their paracrine signalling play important roles in the healing and remodelling of cortical bones [6]. However, periosteum is often damaged during bone fractures by the intense torsion/bending, its tear and detachment preventing normal biological functions to be played out [7]. Crucially, new bone formation only occurs on the perimeter of intact periosteum [8,9]. While grafting of bone fillings/scaffolds are highly prevalent for fracture/osteoporosis treatment within a clinical setting, bone grafts may ultimately fail as the grafted materials lack the support of a functioning periosteum, leading to prolonged inflammation, poor vascular ingrowth, and subsequently inferior bone regeneration [10,11].

As natural periosteum proves difficult to harvest for implant within a clinical setting, research efforts have been placed in the creation of artificial periosteum through engineering means such as cell sheets [12], cell-laden hydrogels [13] and electrospinning [14]. Of which, electrospinning receives particular attention owing to its modular components and ability to generate nanofibers structurally akin to Sharpey's fibres which connects the inner periosteum to bone [15,16]. Additionally, cell sheets and cell-laden hydrogels lack the mechanical properties and cues to serve as a functional periosteum scaffold. Notably, the electrospun fibers express excellent recruitment and guidance of MSCs and

* Corresponding author. Department of Applied Biology and Chemical Technology, the Hong Kong Polytechnic University, Hung Hom, Kowloon, China.
E-mail address: xin.zhao@polyu.edu.hk (X. Zhao).

https://doi.org/10.1016/j.compositesb.2024.111410
Received 15 February 2024; Received in revised form 9 March 2024; Accepted 20 March 2024
Available online 27 March 2024

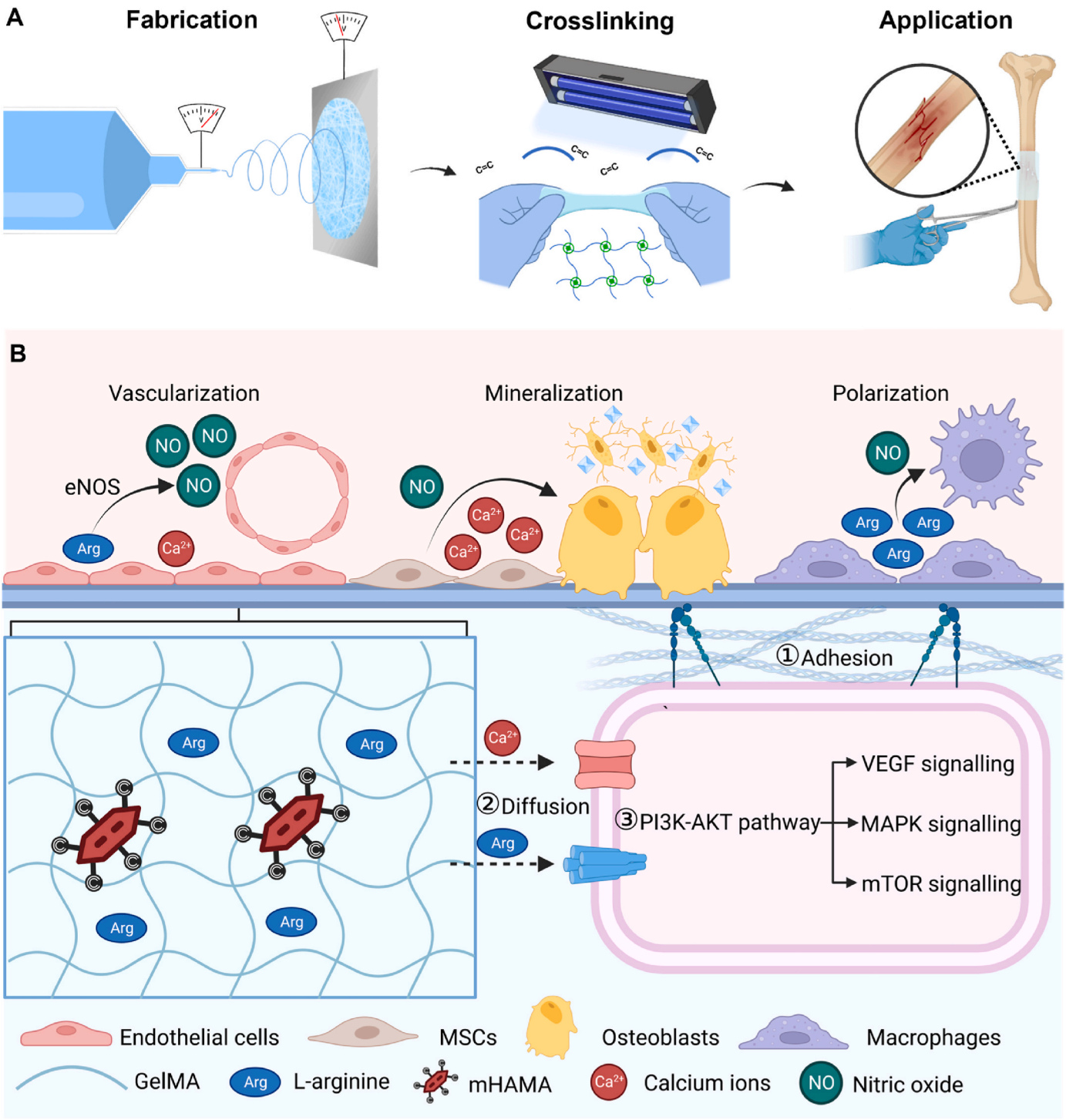

Fig. 1. Schematic depicting application and mechanism of ECM based Ca^{2+}/L-arginine/NO periosteum. (A) Fabrication process of the periosteum scaffolds by electrospinning, photocrosslinking and application to bone fracture sites. (B) Molecular composition and mechanism of action in native cell modulation of periosteum scaffolds. Created with BioRender.com.

endothelial cells (ECs), both of which are essential for osteogenic-angiogenic coupling [17]. Under the principle that bone and blood vessel regeneration go hand in hand, studies have fabricated high performance periosteum scaffolds by electrospinning nanofibers loaded with L-arginine [14]. L-arginine can be converted into nitric oxide (NO) by ECs via endothelial nitric oxide synthase (eNOS), which regulates relaxation of blood vessels, and is an essential biological cue for endothelialization and modulation of the MSCs/ECs paracrine [18,19]. Compared with simple NO-releasing systems, it is particularly important for periosteum to stimulate NO production as the mammalian NO cycle regulated much of the bone homeostasis, serving as the basis for long-term vascular ingrowth, nutrient exchange and cell recruitment to aid in tissue regeneration [19–21]. On the other hand, the immune system has recently been revealed to play a major role in modulating bone regeneration [22,23]. Of note, macrophages stand in the forefront of all host-implant interfaces. They are present in nearly all tissues of the human body to combat pathogens and foreign bodies, and secrete both osteogenic and angiogenic markers as a major mediator of bone healing

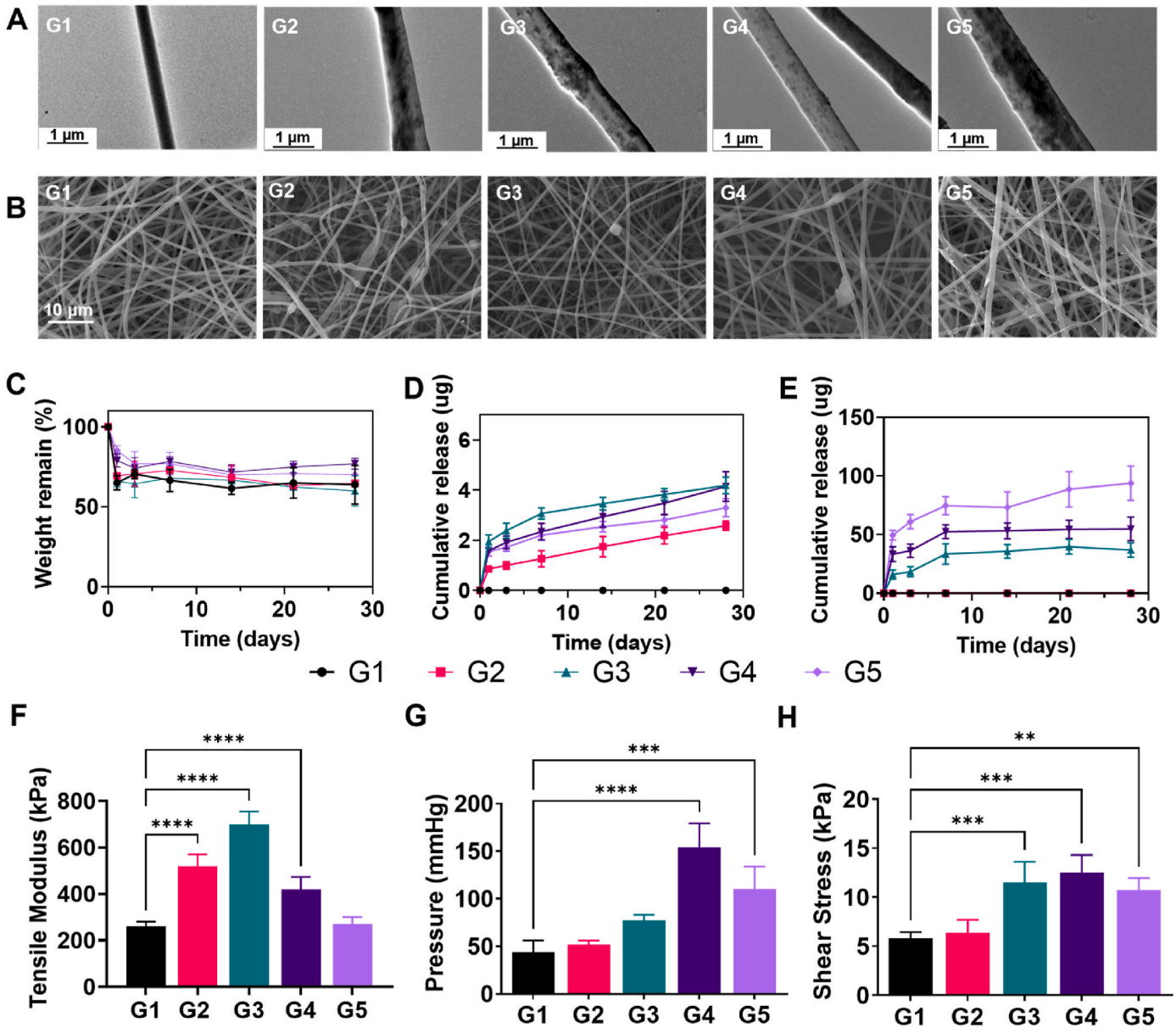

Fig. 2. Characterization of morphology, release kinetics and physical parameters of G1-G5 periosteum scaffolds. (A) SEM and (B) TEM images of G1-G5 periosteum scaffolds. (C) Degradation, (D) Ca^{2+} release and (E) L-arginine release of G1-G5 periosteum scaffolds immersed in PBS over 28 days. (F) Tensile modulus, (G) burst pressure and (H) lap shear properties of G1-G5 periosteum scaffolds reconstituted with water by immersion over 1 h.

[24,25]. The polarization of macrophage towards M2 phenotypes is shown to contribute towards anti-inflammatory healing [26,27]. Interestingly, macrophages can partially contribute towards conversion of L-arginine to NO via inducible nitric oxide synthase (iNOS), and higher concentrations of L-arginine induces macrophage gravitation towards M2 phenotypes via arginase metabolism, which greatly aids in bone regeneration since prolonged inflammation at the fracture site exerts oxidative stress on surrounding cells, inhibits osteoblast maturation and attenuates healing [28,29]. Despite the extensive claim of utilizing macrophage polarity in bone regeneration, few studies systematically elucidated the mechanism of periosteal macrophage in bone regeneration.

Here, we propose a methacrylated gelatin (GelMA)/mesoporous methacrylated hydroxyapatite (mHAMA)/L-arginine electrospun periosteum to promote bone regeneration through osteogenic-angiogenic coupling and macrophage modulation mediated by NO cycle (Fig. 1A). The bulk of spinning solution consists of photocrosslinkable GelMA, a derivative of collagen which is an essential component of the extracellular matrix (ECM) [30–33]. The abundant arginine-glycine-aspartic acid (RGD) sequences enables cell-ECM interactions such as cell adhesion, motility and matrix remodelling. mHAMA nanoparticles possess superior interfacial interact-ability thanks to their increased surface area, sustainably releasing calcium ions (Ca^{2+}) to stimulate bone regeneration and catalysing many intracellular functions including eNOS [34,35]. GelMA and mHAMAs intercrosslink under ultraviolet radiation (UV) to reinforce the hybrid crosslinking density of the polymer network while addition of L-arginine increases water sorption and tissue adhesiveness of the scaffolds [14,36]. L-arginine also serves as a bulk NO precursor, upregulating the expression of eNOS to modulate paracrine cell behaviour. Upon application of periosteum scaffolds to the fracture site, native macrophages first come into contact with the scaffolds and activate M2 polarity after exposure to the high concentrations of L-arginine (Fig. 1B). The recruited ECs from the fracture exudate combined with the released Ca^{2+} then upregulate the eNOS,

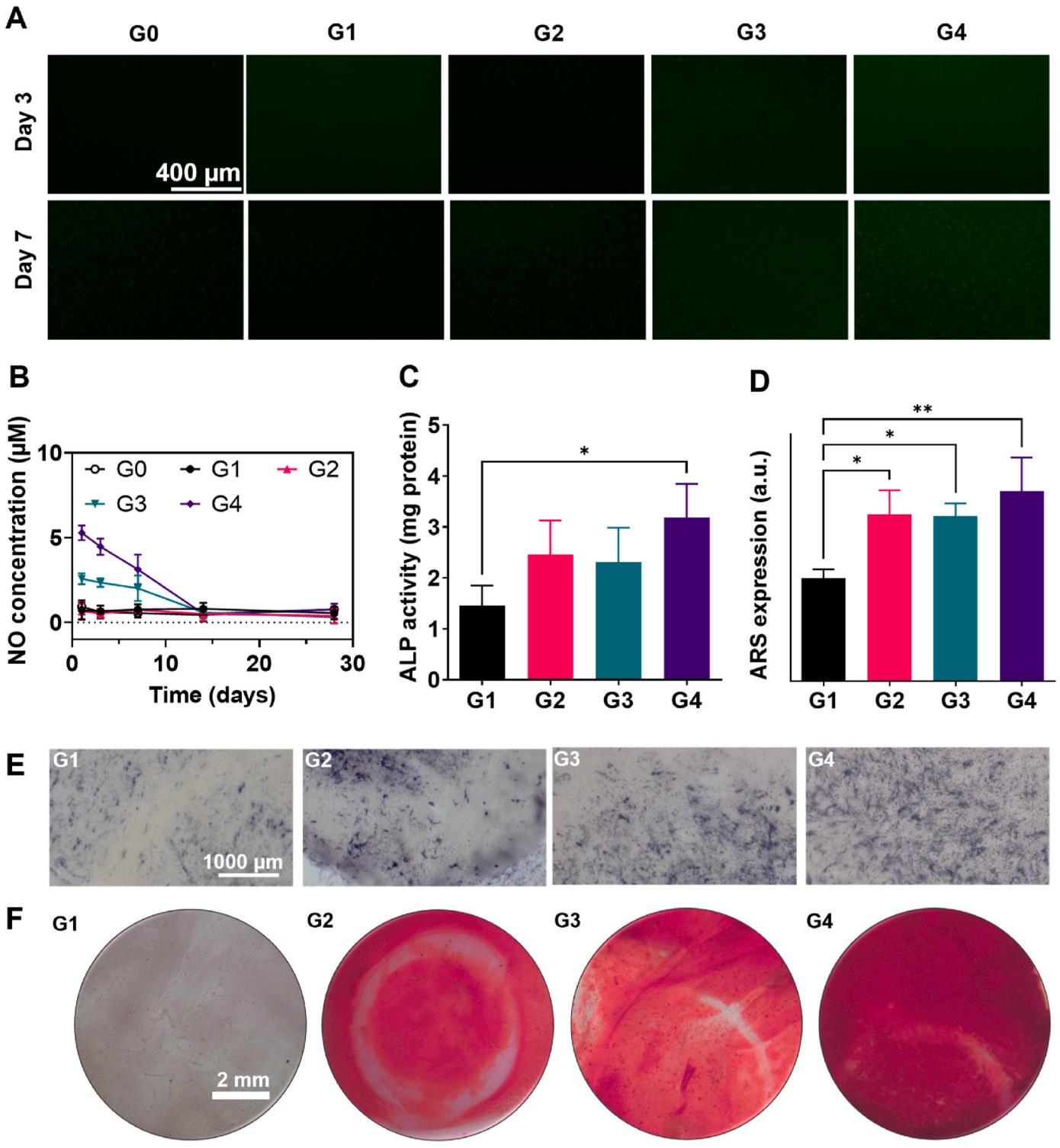

Fig. 3. Characterization of osteogenesis efficacy of G1-G4 periosteum scaffolds by MSC seeding. (A) NO probe images on days 3, 7 and (B) quantification of NO generation in MSCs on periosteum scaffolds over 28 days. (C) Quantification of (E) ALP staining in periosteum scaffolds on day 3. (D) Quantification of (F) ARS staining in periosteum scaffolds on day 7.

initiating VEGF signalling for endothelialization and converting L-arginine to NO for activation of the mTOR pathway by phosphorylation, which consolidates the anti-inflammatory M2 phenotype of macrophages. Finally, the activation of downstream MAPK and ERK signalling by NO and Ca^{2+} via the PI3K-AKT pathway upregulates the cell survival/proliferation and osteogenesis in the complex matrix of periosteum microenvironment, enhancing MSC differentiation into osteoblasts and deposition of mineralized tissues for enhanced bone regeneration. Here, we fully elucidate the mechanism of NO cycle within the multifaceted network of the PI3K-AKT pathway within a bone fracture setting, spanning over osteogenesis, angiogenesis and macrophage polarization mediated by a stiff, adhesive and naturally metabolizable Ca^{2+}/L-arginine/NO periosteum scaffold, with simple and clean clinical translation and implications for anti-inflammatory healing.

2. Results and discussion

2.1. Synthesis and characterisation of mHAMA

Mesoporous hydroxyapatite (mHA) was synthesized through templating of CTAB and sintering. The resultant particles exhibited the characteristic rod shape of hydroxyapatite minerals under TEM, with roughly 20 nm width and 50–100 nm length as well as visible mesopores distributed among its surfaces (Fig. S1). After confirming the morphology of the mHA nanoparticles, we moved on to functionalizing them with methacrylate groups for photocrosslinkability. After reaction with short HEMA chains, we confirmed the functionalization of methacrylate groups onto the mHA surface by FTIR. An increase in C═O peak at 1750 nm was observed, indicating the successful conjugation of HEMA onto mHA, denoted as mHAMA. TGA analysis showed that mHAMA contained around 70% of dry weight in organic matter, which combusted at around 300°C. XRD analysis showed an elevation in intensity near 20° 2θ, which was iconic of XRD pattern of poly(methyl methacrylate) [37]. These results collectively showed the successful functionalization of C═C groups on the surface of mHAMA, which was essential for photocrosslinkability. BET analysis showed that mHA and HA exhibit distinct pore distributions. While the mHAMA showed a shift in pore size, they were able to maintain their mesopores after the chemical modification. We hypothesized that the functionalization of HEMA on mHAMA surface altered the aggregation behaviour of the nanorods, leading to increased distance between each nanoparticle. Thus, these results indicated that we have successfully synthesized and functionalized mHAMA nanoparticles with well-established morphology and composition, and were available to be used in electrospinning.

After well dispersing the mHAMA particles in the spinning solution by sonication, periosteum scaffolds G1-G5 were fabricated (see Table S1). For all groups, consistent fiber formation was observed where 20 mM of L-arginine was the highest concentration achievable while being consistently spinnable. TEM imaging of the scaffolds revealed that mHAMA was well distributed within G2-G5 lumen, while the addition of L-arginine did not significantly increase the diameter of G3-G5 electrospun fibres despite an increase in solution viscosity (Fig. 2A). The consistent fiber formation could be observed in SEM images of the scaffolds, where multiple layers of fibers were distinctly stacked (Fig. 2B). After crosslinking with 10% w/v of IR2959 in ethanol and reaching swelling equilibrium in PBS, the interlinked fibers maintained their morphology despite rehydration and swelling (Fig. S2). For all groups, the crosslinked membranes exhibited densely white appearance with good elasticity and stiffness. We then proceeded to assess the release kinetics and physical properties of the working periosteum scaffolds (Fig. 2 C-E). Degradation tests revealed that the scaffolds maintained well over 60% of its original weight after 28-day incubation in PBS solution, while they experienced an initial burst release of around 8.77 ± 0.81% Ca^{2+} and 13.91 ± 2.61 % L-arginine before sustainably releasing 23.03 ± 3.18 % and 22.9 ± 4.18 % respectively over 28 days. This showed that the periosteum scaffolds were able to maintain the physical shape and support the bone regenerative process over a long period of time. Next, our scaffolds were mechanically assessed through simple tensile tests. The addition of mHAMA greatly increased the tensile modulus of the scaffolds at as high as 800 kPa, while the lower concentrations of L-arginine proved to be more effective at further increasing the stiffness of the scaffolds, making it comparable to the natural periosteum's 0.92–1.93 MPa [38]. However, a drop in the mechanical properties was observed in G5, suggesting that L-arginine provided an increase in tensile modulus only up to 10 mM. In burst pressure and lap shear tests, L-arginine has been shown to increase the adhesiveness of the scaffolds. This was partly owing to its ionic interactions between different components of the scaffolds and with charged surfaces such as natural porcine membranes. Particularly, 10 mM of L-arginine was able to increase the average burst pressure by 3-fold (up to 154.44 ± 24.59 mmHg) and shear strength by 2-fold (up to 12.48 ± 1.82 kPa) respectively. This was especially crucial for periosteum implants as the scaffolds would be required to attach onto the fracture site under wet physiological conditions and withstand fluid pressures leading to potential detachment [39], while supporting the new bone regeneration through biophysical cues. These results showed that electrospinning and UV crosslinking in organic solvent was an effective method of creating ECM based Ca^{2+}/L-arginine nanofibrous periosteum scaffolds. Owing to the high concentration of 20 mM L-arginine leading to a significant drop in the mechanical properties of G5, we selected G1 to G4 for the following experiments.

2.2. Biocompatibility assessments of periosteum scaffolds

With the bulk mechanical properties of our periosteum scaffolds established, we then characterized the cytocompatibility and bioactivity of our scaffolds. First, cell viability test was performed as a general assessment of the cytotoxicity of our different groups, with MSCs as a model cell for bone, HUVECs for endothelium and RAW 264.7 macrophage for immune system (Fig. S5). For all groups on day 1 and day 3, over 95% viability was observed for MSCs, HUVECs and RAW 264.7s. Similar results were observed in cell proliferation assay of the scaffolds, where all groups were able to maintain similar or increased metabolic activities compared to control. While GelMA was well established in terms of biocompatibility, these tests showed that the addition of mHAMA and L-arginine do not induce cytotoxicity to surrounding cells. Additionally, all model cell types were able to adhere onto the scaffolds and exhibit spreading morphology, showing that the scaffolds can well support the attachment and proliferation of both cell types (Fig. S6). Particularly, pseudopodia was observed in macrophages seeded on G4 scaffolds, suggesting increased activation of macrophage phenotypes on these samples [40]. All in all, the abundant RGD motifs of GelMA and the ECM-mimetic nanofibrous structure of our periosteum scaffolds proved sufficient for support of essential cell types in bone regeneration.

2.3. NO generation and osteogenic differentiation of MSCs on periosteum scaffolds

Next, we characterized the periosteum scaffolds' capabilities for stimulating bone growth with the aid of NO production from the periosteum scaffolds. NO generation by periosteum scaffolds was first quantified using NO probe, showing that G3 and G4 groups expressed elevated NO production in the first week of culture (Fig. 3A and B). Notably, owing to the active depletion of L-arginine by MSCs to generate NO, the release of NO was much quicker than the passive release of L-arginine in Fig. 2E. To investigate the effects of NO on the initiation of osteogenesis, ALP staining was performed on MSCs seeded on the scaffolds to assess the early onset of osteogenesis (Fig. 3E). On day 7, dark blue precipitates were clearly visible on the attached MSCs to the scaffolds. Notably, denser and darker mineral clusters could be observed in G2-G4. Quantifying ALP expression in these scaffolds further showed that mineralization in G2-G4 significantly increased, with G4 nearly doubling the calcium deposits of G1. This suggested that the presence of mHAMA nanoparticles was able to contribute towards better early osteogenesis, which corresponded well to other studies which documented the effect of hydroxyapatites and ceramics on osseointegration and bone regeneration [41]. To investigate the effects of late osteogenesis in the periosteum scaffolds, ARS assay was performed (Fig. 3F). While very little mineralization was observed in G1, rich mineralization of calcium indicated by the emergence of red precipitates were observed in G2-G4. Notably, G4 exhibited the highest absorbance corresponding to calcium deposits compared to other groups, which indicated that appropriate concentration of L-arginine and the strongest overall mechanical properties of G4 may also contribute towards late-stage osteogenesis. These findings corresponded with another study on the

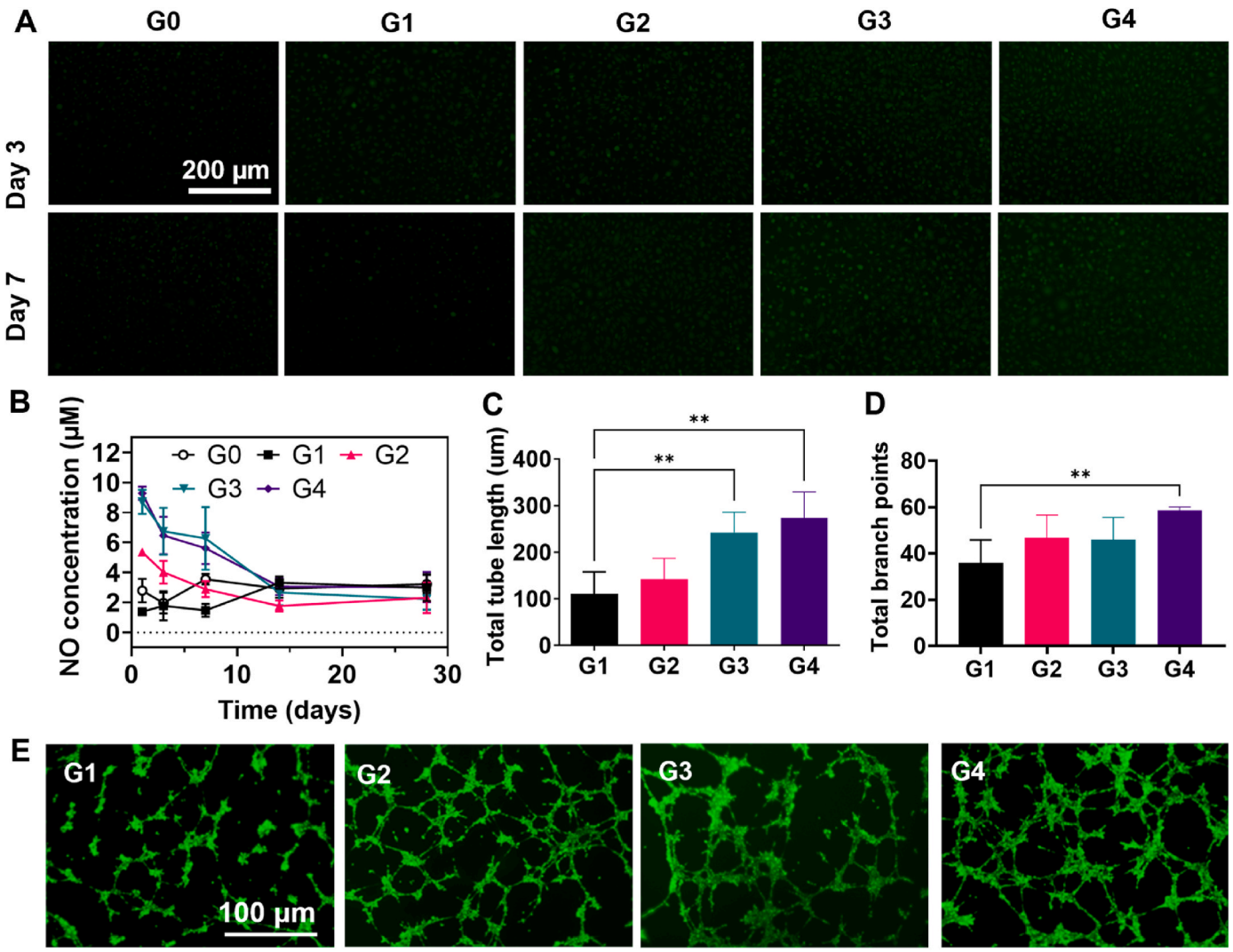

Fig. 4. Characterization of angiogenic efficacy of G1-G4 periosteum scaffolds by HUVEC seeding. (A) NO probe image on days 3, 7 and (B) quantification of NO generation in HUVECs on periosteum scaffolds over 28 days. Quantification of (C) tube length and (D) total branch points of HUVECs seeded on scaffolds for tube formation assay. (E) Representative images of tube formation assay on periosteum scaffolds.

less-documented effect of L-arginine on osteogenesis, where 1 μM L-arginine alone was able to significantly increase the expression of both ALP and ARS of MSCs even in a biofilm setting [42]. Hence, we could conclude that our mHAMA laden G2-G4 periosteum scaffolds were able to elevate both early and late osteogenesis for bone healing, with G4 (with 10 mM L-arginine) displaying the best performance.

2.4. NO generation and angiogenesis of HUVECs on periosteum scaffolds

After assessing the osteogenic capabilities of our periosteum scaffolds, we moved on to the angiogenic assessment for its implications for bone regeneration. First, we quantified the NO production of HUVECs seeded on the scaffolds using NO probe (Fig. 4A and B). We observed that the addition of mHAMA and L-arginine both significantly contributed towards NO production. We attributed the improved NO secretion to the calcium ions present in mHAMAs, which catalysed the conversion of L-arginine into NO via the eNOS pathways [18]. Through the supply of catalysts and substrates for NO production, our scaffolds were able to increase the NO concentrations within the surrounding microenvironments, which were reported to promote angiogenic activity and endothelium regeneration [43]. This was reflected in the observations seen in tube formation assay, where the onset of endothelial formation was prominently increased by L-arginine concentration (Fig. 4E). In G1, despite the lack of NO-production cues, visible networks and interlinkage between HUVEC clusters were developing, showing the endothelial compatibility of GelMA. However, the inclusion of mHAMA and especially 5 mM and 10 mM L-arginine significantly increased both the branch points and total tube length of the seeded HUVECs, which was evidence of endothelial growth (Fig. 4C and D). These results showed a strong connection between Ca^{2+} and L-arginine with blood vessel formation, and indicated that our periosteum was able to stimulate endothelium formation through its bioactive components.

2.5. NO generation and polarization of macrophages on periosteum scaffolds

Recent studies had shown the role of macrophages as a powerhouse to mediating bone regeneration. The depletion of macrophages in animal models led to impaired bone reunion and fibrotic changes [44,45], while macrophage involvement in both vascular growth and osteoblastic differentiation were clarified, in addition to their implications for inflammatory and anti-inflammatory phenotypes [46–48]. Notably, macrophages had been recorded to often express both M1-like and M2-like cytokines, suggesting the clear-cut polarization of M1/M2 to be oversimplified [49,50]. Bearing this in mind, we first assessed the NO generation of macrophages seeded on the scaffolds, which showed that

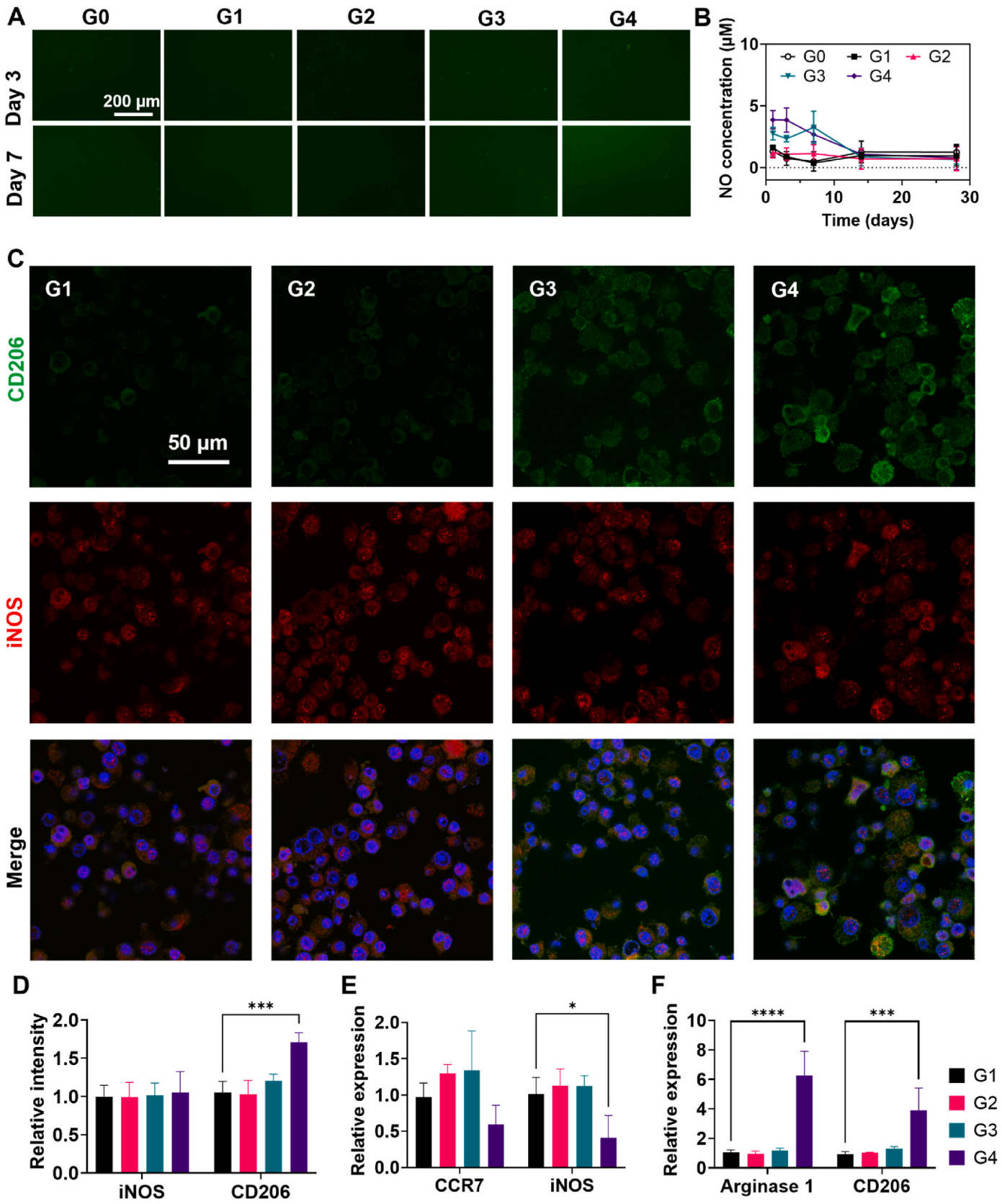

Fig. 5. Characterization of immunomodulating efficacy of the G1-G4 periosteum scaffolds by RAW264.7 seeding. (A) NO probe image on days 3, 7 and (B) quantification in periosteum scaffolds over 28 days. (C) Immunostaining images and (D) fluorescence quantification of RAW264.7 with iNOS and CD206 markers. qPCR expression of (E) M1 markers CCR7, iNOS and (F) M2 markers Arginase 1, CD206 of RAW264.7 seeded on periosteum scaffolds.

Table 1
Classification of macrophage polarization based on flow cytometry fluorescence levels of iNOS and CD206 markers on RAW264.7 co-cultured with periosteum scaffolds.

Group	$iNOS^{-}/CD206^{-}$ (%)	$iNOS^{+}/CD206^{-}$ (%)	$iNOS^{-}/CD206^{+}$ (%)	$iNOS^{+}/CD206^{+}$ (%)
G1	68.1	18.3	6.29	7.29
G2	61.1	23.9	5.04	9.99
G3	53.8	25.6	3.57	17.1
G4	56.2	15.7	8.99	19.1

G3 and G4 groups displayed elevated NO concentration during the first week (Fig. 5A and B). NO had been revealed to largely influence the behaviours of macrophages owing to its inherent ability to utilize NO as a defence mechanism against pathogens [51]. Next, we explored the influence of periosteum scaffolds on its surrounding macrophages through immunostaining of M1 (iNOS) and M2 (CD206) markers, which were iconic surface markers of macrophages where their elevated expression each signifies a polarization phenotype (Fig. 5C and D). While no significant differences in M1 expression were observed between all groups of periosteum, G4 expressed enhanced M2 expression presumably because of the presence of high concentration L-arginine, as it induced the expression of arginase in macrophages to degrade L-arginine into metabolic products [52]. To confirm this hypothesis, we verified our results using qPCR of M1 macrophage markers CCR7 and iNOS with M2 markers Arginase 1 and CD206 (Fig. 5E and F) [53]. We found that G4 exhibited lowered iNOS expression, suggesting a downregulation of M1 polarization of macrophages on these scaffolds; whereas G4 displayed both enhanced Arginase 1 and CD206 expression, which showed that M2 polarization was upregulated. Additionally, owing to the limited range in the fluorescence intensities of M1 and M2 markers in the confocal images, we further performed flow cytometry with M1 (iNOS) and M2 (CD206) markers to assess the condition of macrophages as they could be expressing both or none of the polarized phenotypes (Table 1). The addition of mHAMA seemed to increase the expression of M1 macrophages, while L-arginine increased the M2 macrophages in a dosage dependent manner from 6.29% to 8.99% for the $iNOS^{-}/CD206^{+}$ group and from 7.29% to 19.1% for the $iNOS^{+}/CD206^{+}$ group. Additionally, L-arginine was able to decrease the proportion of macrophages that express only M1 phenotypes from 23.9% to 15.7%, confirming our hypothesis that the presence of L-arginine upregulates M2 polarization and downregulates M1 polarization of macrophages. Together, the bioactive components of the periosteum scaffolds were able to influence the M2 phenotype expression of seeded macrophages, with implications for improved anti-inflammation for bone healing.

2.6. *In vivo osteogenesis efficacy of periosteum scaffolds*

Rat calvarial critical defect was chosen to assess the regenerative efficacy of the periosteum scaffolds. Reconstructed CT scans showed that different groups had achieved differing degrees of bone regeneration of rat cranial tissues (Fig. 6A). Notably, G4 exhibited significantly improved BMD at 0.378 ± 0.051 g/cm^3 (~2.42 fold of G0), BV/TV at 37.80 ± 8.65% (~2.54 fold of G0) and bone thickness at 294.75 ± 58.03 μm (~1.99 fold of G0) at week 8 (Fig. 6 B-D). G4's overall bone healing performance was also visibly the most satisfactory with nearly enclosed skull tissues at week 8. Meanwhile, H&E and Masson's Trichrome staining of cranial tissue slices showed both the highest formation and thickness of matured bone tissues on the cranial tissues treated by G4 compared to other groups (Fig. 6E). This showed that both the quality and quantity of new bone formation of G4 outperformed other groups, paralleling the *in vitro* osteogenesis assessment results, where a sufficient concentration of L-arginine showed the best bone mineralization. We hypothesize that the generated NO, L-arginine and the released calcium ions from the periosteum scaffold could nourish the bone microenvironment and enhance the mineralization of regenerating tissues, leading to the improved new bone formation and quality.

2.7. *Mechanism of osteogenesis of periosteum scaffolds*

To investigate the working mechanism behind the heightened bone formation in periosteum scaffolds, G1, G2 and G4 were chosen to conduct the whole organism RNA sequencing based on their difference in components to systematically evaluate the therapeutic effects of mHAMA and L-arginine. Pearson Correlation of sample groups showed low within-group variance, suggesting good sample stability and consistency (Fig. S8A). The Venn diagram and volcanic plot of these 3 groups showed distinct differences in hundreds of genes, suggesting that there were fundamental differences in the expressed genes owing to the scaffold implant (Fig. 7A and B). The heatmap further supports this observation, where G1, G2 and G4 expressed different upregulated and downregulated genes within regenerative pathways (Fig. 7C). To pinpoint the genetical changes in sample groups, the significantly upregulated and downregulated genes were first filtered using relevant keywords related to osteogenesis, angiogenesis and immune system, then processed using GO terms and KEGG pathway analysis (Fig. 7D and E). Notably, GO terms of G4 expressed upregulation of calcium ion and collagen binding, blood vessel development and ion channel activity, suggesting that its improvement in bone mineralization lied in the improved calcium ion activity in cells. KEGG analysis further showed an upregulation of upstream molecules such as integrin A and G protein-coupled receptors in the PI3-AKT pathway, which was a broad signalling pathway regulating multiple cellular processes involving cell proliferation, osteogenesis, angiogenesis (Fig. S9) [54,55]. The surface interactions between adherent cells and the periosteum scaffolds by ECM components might lead to activation of downstream molecules in the pathway. Strong evidence of PI3-AKT pathway modulation of macrophages was also widely reported [56,57]. Additionally, KEGG analysis of G4 vs G2 showed upregulation of MAPK, Ras and Rap1 signalling pathway, all of which are intermediate pathways within PI3-AKT, as well as increased endothelium and blood vessel development in GO terms (Figs. S8D and E). These RNA sequencing results suggested favourable regulation of expressed genes in the PI3K-AKT pathway of G4 compared to G1 and G2.

However, the relatively low number of genes shown in the KEGG analysis could only suggest weak relation to the listed pathways. Here to confirm our hypothesis, noteworthy downstream molecules and effectors of the PI3-AKT pathway were chosen to be quantified by qPCR (Fig. 8A and B). Key signalling molecules within the pathway including PDK1, AKT, ras, rap1, ERK1/2 and p38 MAPK were all significantly upregulated in G4 compared to G1. These results justified the claim that the PI3K-AKT pathway was the major player leading to enhanced bone regeneration. Additionally, the downstream effectors VEGF, eNOS, HIFα for angiogenesis and OSX, Runx2, OCN for osteogenesis were both significantly upregulated in G4, further reinforcing the mechanism of action. Notably, inflammatory molecules TNF and IL-17 were downregulated while mTORC1 was significantly upregulated in G4, showing that the presence of L-arginine, generated NO and the subsequent influence of the mTOR pathway on the M2 polarization of macrophages were able to achieve anti-inflammatory effects in bone repair. All in all, the qPCR results showed that our periosteum scaffolds activated the PI3K-AKT signalling and led to the downstream action of VEGF, MAPK

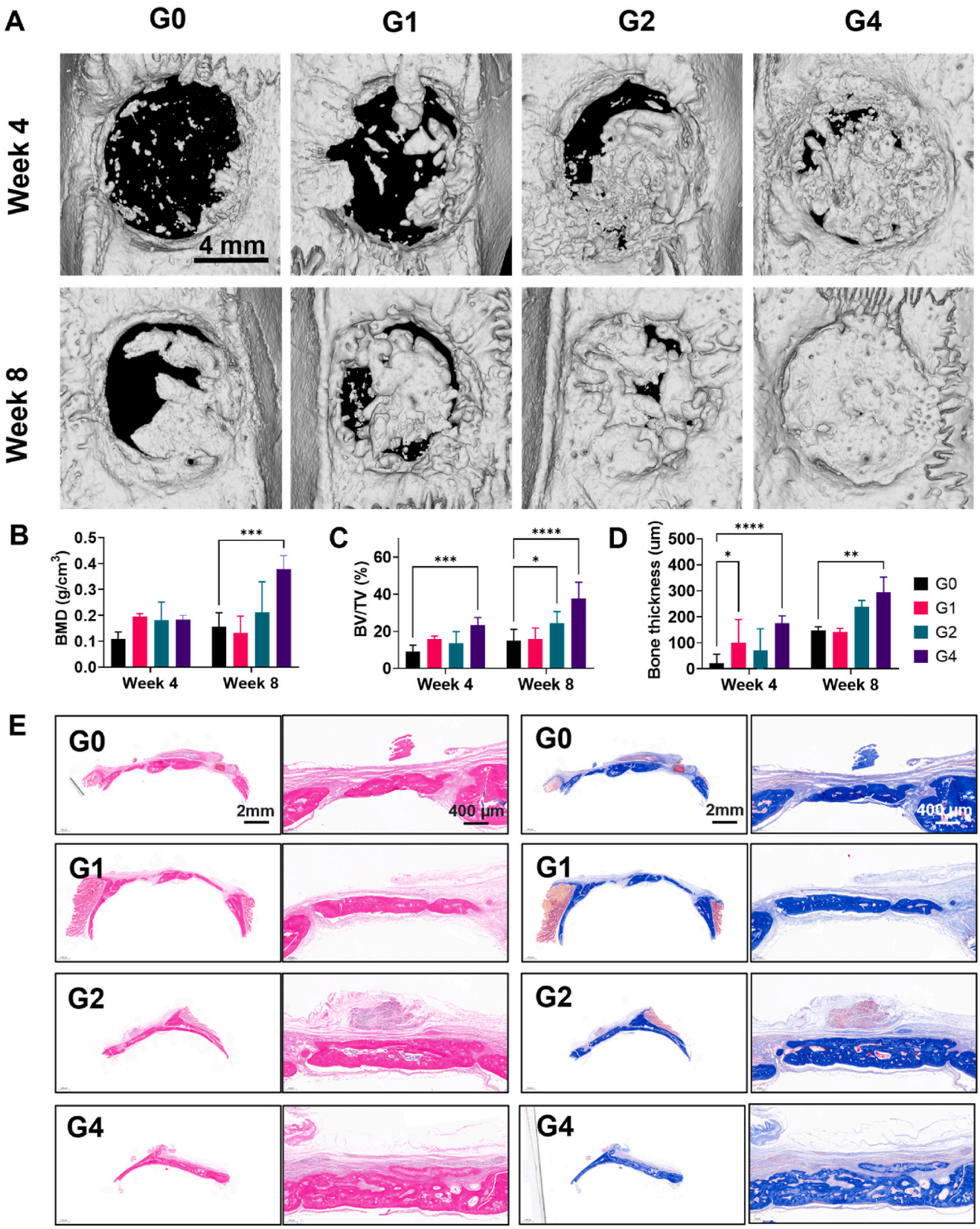

Fig. 6. *In vivo* characterization of bone regenerative efficacy of G0 (no treatment), G1, G2, and G4 periosteum scaffold implants in a rat calvarial critical defect model. (A) Reconstructed CT images, (B) BMD, (C) BV/VT and (D) quantified bone thickness of cranial tissues 4 and 8 weeks post-surgery. (E) H&E (pink = soft tissues; magenta = hard tissues) and Masson's Trichrome (light blue = soft tissues; dark blue = hard tissues) staining of cranial tissue slices of cranial tissues 8 weeks post-surgery.

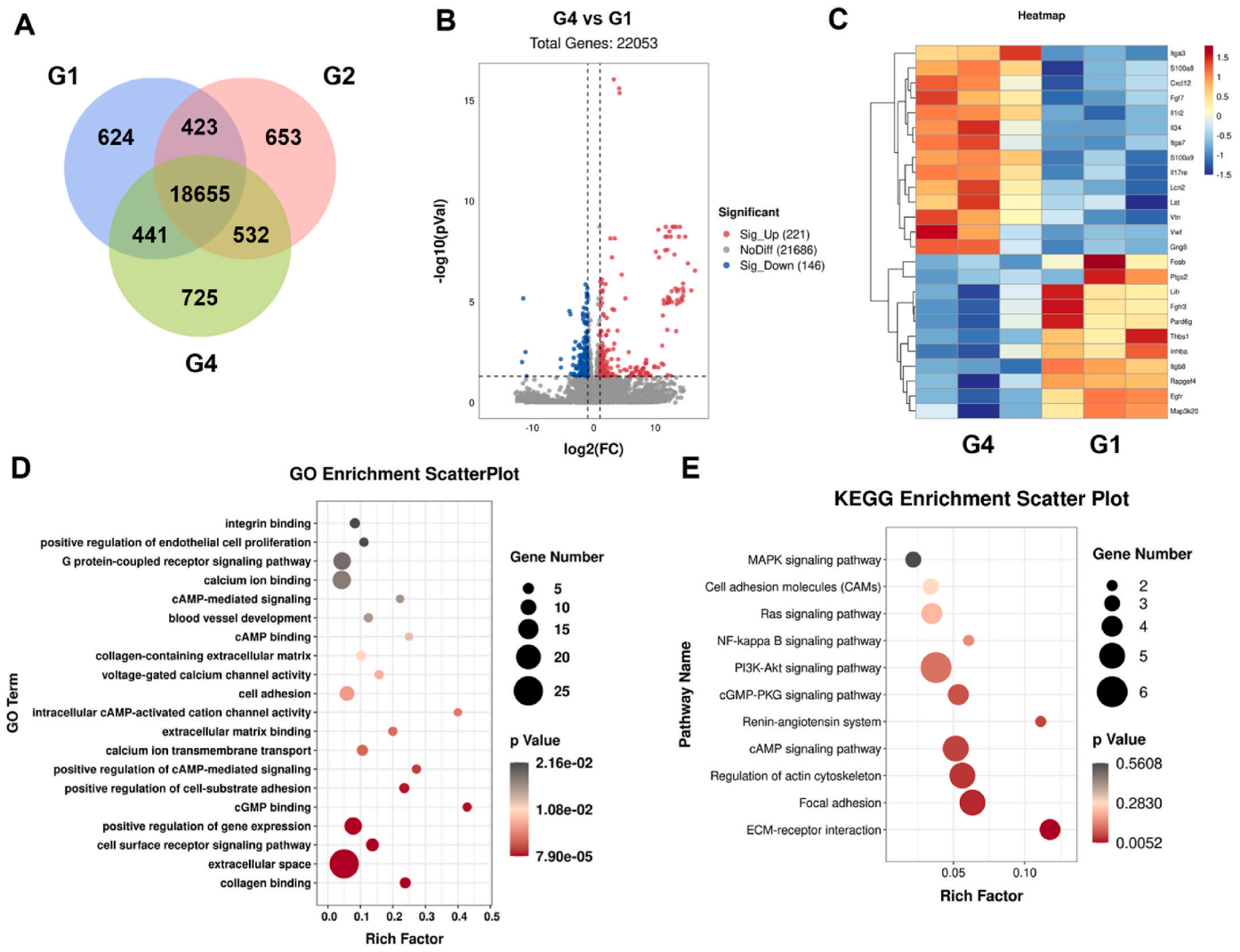

Fig. 7. RNA sequencing of G1, G2 and G4 cranial tissue samples. (A) Venn diagram of expressed genes between G1, G2 and G4. (B) Volcano Plot, (C) gene heat map, (D) top 20 functions in GO enrichment and (E) top 10 pathways in KEGG enrichment of G4 vs G1 after filtering by relevant keywords related to osteogenesis, angiogenesis and immune system. The results showed broad elevation in expression for calcium binding, endothelial growth, cell adhesion and upregulated pathways under the PI3K-AKT interactive signalling.

and mTOR pathways for angiogenesis, osteogenesis and macrophage polarization (Fig. 8C).

We have demonstrated the relationship between NO, L-arginine, calcium ions and the upregulated PI3K-AKT pathway with bone regeneration. The PI3K-AKT pathway is a multifaceted cellular concourse that modulates many downstream functions that benefits bone regeneration, interlinked by influences from free radical NO. The released L-arginine and calcium ions from periosteum scaffolds could enter the cytoplasm of native cells via hCAT-1 and ion channels respectively, and contribute towards sustaining the NO production by eNOS [58]. The process depleted dissolved oxygen and upregulated HIF-1α and VEGF, feeding back to upregulation of PI3K molecule, which was also activated by stimulation of laminin and integrin A by cell attachment to periosteum scaffold surface. From there, AKT further upregulated the activity of eNOS, which generated ample NO to phosphorylate mTORC1 for modulation of macrophage polarization, as well as activating the ERK1/2 signalling alongside ras and rap1 pathways for cell survival [59,60]. Notably, NO and macrophage activity was inextricably linked to osteogenesis: NO could upregulate the activity of ALP, OCN and bone sialoprotein (BSP) for improved bone healing while macrophages treated with NO express anti-inflammatory phenotypes and enhanced neovascularization [61]. This combined with the enhancement of Runx2 transcription and osteoblast differentiation of MSCs by AKT signalling led to synergistic enhancement of bone regeneration. All in all, the permeated action of Ca^{2+}/L-arginine/NO periosteum could kickstart the activation of the PI3K-AKT pathway, leading to synergistically enhanced osteogenesis, angiogenesis, and macrophage polarization. This is the first study to demonstrate that the PI3K-AKT pathway could be comprehensively initiated by eNOS through the synergistic actions of a Ca^{2+}/L-arginine/NO periosteum scaffold, encompassing intricate cellular signalling including RUNX2, MTORC and ERK1/2 pathways to direct native cells towards osteogenesis.

3. Conclusion

We fabricated ECM based Ca^{2+}/L-arginine/NO periosteum scaffolds and studied their performance and mechanism of action *in vitro* and *in vivo*. The scaffolds loaded with mHAMA and L-arginine displayed excellent mechanical properties and long-term release of Ca^{2+} and L-arginine. Moreover, the ECM based Ca^{2+}/L-arginine periosteum scaffolds were able to induce NO generation in multiple cell types, leading to enhanced bone mineralization, vascularization and macrophage polarization. Rat calvarial critical defect models revealed significantly enhanced new bone formation and quality, as well as synergistic action

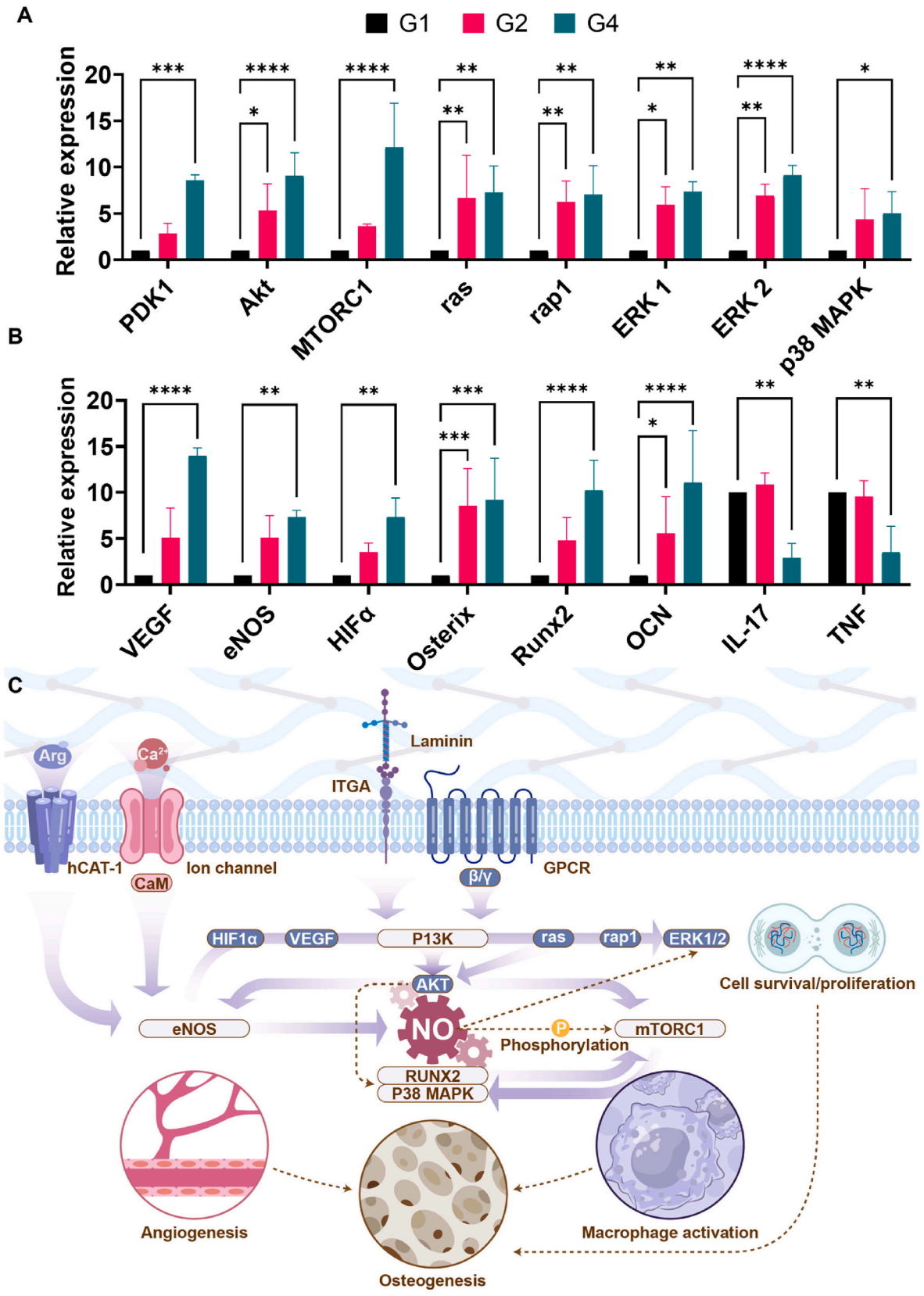

Fig. 8. The PI3K-AKT pathway and its relation to osteogenesis, angiogenesis and immunomodulation. qPCR of (A) notable intermediate molecules within the PI3K-AKT pathway, (B) angiogenic genes, osteogenic genes and pro-inflammatory molecules in rat cranial tissues implanted with periosteum scaffolds. (C) Schematic depicting the crosstalk between molecules within the PI3K-AKT pathway leading to tissue functions.

of VEGF, MAPK and mTOR pathway via NO cycle within the signalling concourse of the PI3K-AKT signalling.

CRediT authorship contribution statement

Ho-Pan Bei: Writing – review & editing, Writing – original draft, Visualization, Validation, Software, Resources, Methodology, Investigation, Formal analysis, Data curation, Conceptualization. **Xiongfa Ji:** Visualization, Validation, Resources, Methodology, Investigation, Funding acquisition, Formal analysis, Data curation. **Tianpeng Xu:** Visualization, Validation, Methodology, Investigation, Data curation. **Zhenhua Chen:** Visualization, Validation, Methodology, Investigation, Data curation. **Chun-Hei Lam:** Visualization, Validation, Methodology, Investigation, Data curation. **Xintong Zhou:** Writing – review & editing. **Yuhe Yang:** Visualization, Validation, Funding acquisition, Formal analysis. **Yu Zhang:** Visualization, Validation, Resources. **Chunyi Wen:** Validation, Visualization. **Yaxiong Liu:** Validation, Visualization. **Xin Zhao:** Writing – review & editing, Writing – original draft, Visualization, Validation, Supervision, Resources, Project administration, Investigation, Funding acquisition, Formal analysis, Conceptualization.

Declaration of competing interest

The authors declare that they have no known competing financial interests or personal relationships that could have appeared to influence the work reported in this paper.

Data availability

Data will be made available on request.

Acknowledgements

This work was supported by the grant from the Guangdong Basic and Applied Basic Research Foundation (2020B1515130002, 2023A1515011544), China the National Science Foundation of China (NSFC) (82122002, 32101097, 82202693), China the Collaborative Research Fund (Grant C5044-21G) from the Research Grants Council (RGC) of Hong Kong, Hong Kong SAR, China, NSFC/RGC Joint Research Scheme (N_PolyU526/22) from the Research Grants Council (RGC) of Hong Kong, Hong Kong SAR, China and the the Innovation and Technology Fund from the Innovation and Technology Commission (Grant no. ITS/085/21), Hong Kong SAR, China.

Appendix A. Supplementary data

Supplementary data to this article can be found online at https://doi.org/10.1016/j.compositesb.2024.111410.

References

[1] Souder C. Temporary structure design. John Wiley & Sons; 2014.
[2] Eltom A, Zhong G, Muhammad A. Scaffold techniques and designs in tissue engineering functions and purposes: a review. Adv Mater Sci Eng 2019;2019.
[3] Collins MN, Ren G, Young K, Pina S, Reis RL, Oliveira JM. Scaffold fabrication technologies and structure/function properties in bone tissue engineering. Adv Funct Mater 2021;31(21):2010609.
[4] Zhang W, Wang N, Yang M, Sun T, Zhang J, Zhao Y, et al. Periosteum and development of the tissue-engineered periosteum for guided bone regeneration. Journal of orthopaedic translation 2022;33:41–54.
[5] Sun Y, Gao Z, Zhang X, Xu Z, Zhang Y, He B, et al. 3D-printed, bi-layer, biomimetic artificial periosteum for boosting bone regeneration. Bio-Design and Manufacturing 2022;5(3):540–55.
[6] Wang X, Thomsen P. Mesenchymal stem cell–derived small extracellular vesicles and bone regeneration. Basic Clin Pharmacol Toxicol 2021;128(1):18–36.
[7] Yang Y, Rao J, Liu H, Dong Z, Zhang Z, Bei H-P, et al. Biomimicking design of artificial periosteum for promoting bone healing. Journal of Orthopaedic Translation 2022;36:18–32.
[8] Xu J, Wang Y, Li Z, Tian Y, Li Z, Lu A, et al. PDGFRα reporter activity identifies periosteal progenitor cells critical for bone formation and fracture repair. Bone research 2022;10(1):7.
[9] Li X, Yang S, Wang S, Li S, Jiang H, Hu W, et al. A hierarchical biomimetic periosteum combined immunomodulatory and osteogenic functions for bone regeneration. Compos B Eng 2022;243:110099.
[10] Sanz-Sánchez I, Sanz-Martín I, Ortiz-Vigón A, Molina A, Sanz M. Complications in bone-grafting procedures: classification and management. Periodontology 2022;88(1):86–102. 2000.
[11] Yang Y, Xu T, Bei HP, Zhao Y, Zhao X. Sculpting bio-inspired surface textures: an adhesive janus periosteum. Adv Funct Mater 2021;31(37):2104636.
[12] Zhang J, Huang Y, Wang Y, Xu J, Huang T, Luo X. Construction of biomimetic cell-sheet-engineered periosteum with a double cell sheet to repair calvarial defects of rats. Journal of Orthopaedic Translation 2023;38:1–11.
[13] Mansoorifar A, Subbiah R, de Souza Balbinot G, Parthiban SP, Bertassoni LE. Embedding cells within nanoscale, rapidly mineralizing hydrogels: a new paradigm to engineer cell-laden bone-like tissue. J Struct Biol 2020;212(3):107636.
[14] Yang Y, Xu T, Zhang Q, Piao Y, Bei HP, Zhao X. Biomimetic, stiff, and adhesive periosteum with osteogenic–angiogenic coupling effect for bone regeneration. Small 2021;17(14):2006598.
[15] Gupta S, Teotia AK, Qayoom I, Shiekh PA, Andrabi SM, Kumar A. Periosteum-mimicking tissue-engineered composite for treating periosteum damage in critical-sized bone defects. Biomacromolecules 2021;22(8):3237–50.
[16] Barbosa F, Ferreira FC, Silva JC. Piezoelectric electrospun fibrous scaffolds for bone, articular cartilage and osteochondral tissue engineering. Int J Mol Sci 2022;23(6):2907.
[17] Maes C, Clemens TL. Angiogenic–osteogenic coupling: the endothelial perspective. BoneKEy Rep 2014;3.
[18] Rao J, Mou X, Mo Y, Bei H-P, Wang L, Tang CY, et al. Gas station in blood vessels: an endothelium mimicking, self-sustainable nitric oxide fueling stent coating for prevention of thrombosis and restenosis. Biomaterials 2023;302:122311.
[19] Tabish TA, Crabtree MJ, Townley HE, Winyard PG, Lygate CA. Nitric oxide releasing nanomaterials for cardiovascular applications. JACC (J Am Coll Cardiol): Basic to Translational Science 2023. https://doi.org/10.1016/j.jacbts.2023.07.017.
[20] Jin Z, Kho J, Dawson B, Jiang M-M, Chen Y, Ali S, et al. Nitric oxide modulates bone anabolism through regulation of osteoblast glycolysis and differentiation. The Journal of clinical investigation 2021;131(5).
[21] Wu G, Meininger CJ, McNeal CJ, Bazer FW, Rhoads JM. Role of L-arginine in nitric oxide synthesis and health in humans. Amino acids in nutrition and health: Amino acids in gene expression, metabolic regulation, and exercising performance 2021:167–87.
[22] Tsukasaki M, Takayanagi H. Osteoimmunology: evolving concepts in bone–immune interactions in health and disease. Nat Rev Immunol 2019;19(10):626–42.
[23] Pazarceviren AE, Evis Z, Dikmen T, Altunbaş K, Yaprakçı MV, Keskin D, et al. Alginate/gelatin/boron-doped hydroxyapatite-coated Ti implants: in vitro and in vivo evaluation of osseointegration. Bio-Design and Manufacturing 2023;6(3):217–42.
[24] Yang C, Zhao C, Wang X, Shi M, Zhu Y, Jing L, et al. Stimulation of osteogenesis and angiogenesis by micro/nano hierarchical hydroxyapatite via macrophage immunomodulation. Nanoscale 2019;11(38):17699–708.
[25] Wei W, Yang R, Yu Q, Zhao J, Li W. Gallium-niobium nanofiber surface of niobium/PEKK composite with anti-inflammatory, osteogenesis and anti-bacterial effects for facilitating osteoblastic differentiation and ameliorating osteointegration. Compos B Eng 2023;248:110375.
[26] Arabpour M, Saghazadeh A, Rezaei N. Anti-inflammatory and M2 macrophage polarization-promoting effect of mesenchymal stem cell-derived exosomes. Int Immunopharm 2021;97:107823.
[27] Xu W-C, Dong X, Ding J-L, Liu J-C, Xu J-J, Tang Y-H, et al. Nanotubular TiO2 regulates macrophage M2 polarization and increases macrophage secretion of VEGF to accelerate endothelialization via the ERK1/2 and PI3K/AKT pathways. International journal of nanomedicine 2019:441–55.
[28] Maruyama M, Rhee C, Utsunomiya T, Zhang N, Ueno M, Yao Z, et al. Modulation of the inflammatory response and bone healing. Front Endocrinol 2020;11:386.
[29] Caputa G, Flachsmann LJ, Cameron AM. Macrophage metabolism: a wound-healing perspective. Immunol Cell Biol 2019;97(3):268–78.
[30] Zhao X, Sun X, Yildirimer L, Lang Q, Lin ZYW, Zheng R, et al. Cell infiltrative hydrogel fibrous scaffolds for accelerated wound healing. Acta Biomater 2017;49:66–77.
[31] Zhao X, Liu S, Yildirimer L, Zhao H, Ding R, Wang H, et al. Injectable stem cell-laden photocrosslinkable microspheres fabricated using microfluidics for rapid generation of osteogenic tissue constructs. Adv Funct Mater 2016;26(17):2809–19.
[32] Zhao X, Lang Q, Yildirimer L, Lin ZY, Cui W, Annabi N, et al. Photocrosslinkable gelatin hydrogel for epidermal tissue engineering. Adv Healthcare Mater 2016;5(1):108–18.
[33] Mei Q, Yuen H-Y, Zhao X. Mechanical stretching of 3D hydrogels for neural stem cell differentiation. Bio-Design and Manufacturing 2022;5(4):714–28.
[34] Wang M, Chen F, Tang Y, Wang J, Chen X, Li X, et al. Regulation of macrophage polarization and functional status by modulating hydroxyapatite ceramic micro/nano-topography. Mater Des 2022;213:110302.
[35] Xun X, Li Y, Ni M, Xu Y, Li J, Zhang D, et al. Calcium crosslinked macroporous bacterial cellulose scaffolds with enhanced in situ mineralization and osteoinductivity for cranial bone regeneration. Compos B Eng 2024;275:111277.
[36] Chen Z, Lv Y. Gelatin/sodium alginate composite hydrogel with dynamic matrix stiffening ability for bone regeneration. Compos B Eng 2022;243:110162.

[37] Abasi CY, Wankasi D, Dikio ED. Adsorption study of lead (II) ions on poly (methyl methacrylate) waste material. Asian J Chem 2018;30(4):859–67.
[38] Zhang W, Sun T, Zhang J, Hu X, Yang M, Han L, et al. Construction of artificial periosteum with methacrylamide gelatin hydrogel-wharton's jelly based on stem cell recruitment and its application in bone tissue engineering. Materials Today Bio 2023;18:100528.
[39] Luo S, Yang L, Zou Q, Yuan D, Xu S, Zhao Y, et al. Rapid suture-free repair of arterial bleeding: a novel approach with ultra-thin bioadhesive hydrogel membrane. Chem Eng J 2023;472:144865.
[40] He F, Umrath F, Reinert S, Alexander D. Jaw periosteum-derived mesenchymal stem cells regulate THP-1-derived macrophage polarization. Int J Mol Sci 2021;22 (9):4310.
[41] Yang Y, Zhang Q, Xu T, Zhang H, Zhang M, Lu L, et al. Photocrosslinkable nanocomposite ink for printing strong, biodegradable and bioactive bone graft. Biomaterials 2020;263:120378.
[42] Noori A, Hoseinpour M, Kolivand S, Lotfibakhshaiesh N, Azami M, Ai J, et al. Synergy effects of copper and L-arginine on osteogenic, angiogenic, and antibacterial activities. Tissue Cell 2022;77:101849.
[43] Jana S. Endothelialization of cardiovascular devices. Acta Biomater 2019;99: 53–71.
[44] Schlundt C, Fischer H, Bucher CH, Rendenbach C, Duda GN, Schmidt-Bleek K. The multifaceted roles of macrophages in bone regeneration: a story of polarization, activation and time. Acta Biomater 2021;133:46–57.
[45] Pajarinen J, Lin T, Gibon E, Kohno Y, Maruyama M, Nathan K, et al. Mesenchymal stem cell-macrophage crosstalk and bone healing. Biomaterials 2019;196:80–9.
[46] Wang Y, Fan Y, Liu H. Macrophage polarization in response to biomaterials for vascularization. Ann Biomed Eng 2021;49:1992–2005.
[47] Muñoz J, Akhavan NS, Mullins AP, Arjmandi BH. Macrophage polarization and osteoporosis: a review. Nutrients 2020;12(10):2999.
[48] Tan J, Zhang Q-Y, Song Y-T, Huang K, Jiang Y-L, Chen J, et al. Accelerated bone defect regeneration through sequential activation of the M1 and M2 phenotypes of macrophages by a composite BMP-2@SIS hydrogel: an immunomodulatory perspective. Compos B Eng 2022;243:110149.
[49] Strizova Z, Benesova I, Bartolini R, Novysedlak R, Cecrdlova E, Foley LK, et al. M1/M2 macrophages and their overlaps–myth or reality? Clinical Science 2023;137 (15):1067–93.
[50] Yao Y, Xu X-H, Jin L. Macrophage polarization in physiological and pathological pregnancy. Front Immunol 2019;10:792.
[51] Palmieri EM, McGinity C, Wink DA, McVicar DW. Nitric oxide in macrophage immunometabolism: hiding in plain sight. Metabolites 2020;10(11):429.
[52] Momma TY, Ottaviani JI. There is no direct competition between arginase and nitric oxide synthase for the common substrate l-arginine. Nitric Oxide 2022;129: 16–24.
[53] Barrett TJ. Macrophages in atherosclerosis regression. Arterioscler Thromb Vasc Biol 2020;40(1):20–33.
[54] Samakova A, Gazova A, Sabova N, Valaskova S, Jurikova M, Kyselovic J. The PI3k/Akt pathway is associated with angiogenesis, oxidative stress and survival of mesenchymal stem cells in pathophysiologic condition in ischemia. Physiol Res 2019;68:S131–8.
[55] Ye C, Zhang W, Hang K, Chen M, Hou W, Chen J, et al. Extracellular IL-37 promotes osteogenic differentiation of human bone marrow mesenchymal stem cells via activation of the PI3K/AKT signaling pathway. Cell Death Dis 2019;10 (10):753.
[56] Linton MF, Moslehi JJ, Babaev VR. Akt signaling in macrophage polarization, survival, and atherosclerosis. Int J Mol Sci 2019;20(11):2703.
[57] Vergadi E, Ieronymaki E, Lyroni K, Vaporidi K, Tsatsanis C. Akt signaling pathway in macrophage activation and M1/M2 polarization. J Immunol 2017;198(3): 1006–14.
[58] Leung WK, Gao L, Siu PM, Lai CW. Diabetic nephropathy and endothelial dysfunction: current and future therapies, and emerging of vascular imaging for preclinical renal-kinetic study. Life Sci 2016;166:121–30.
[59] Covarrubias AJ, Aksoylar HI, Horng T. Control of macrophage metabolism and activation by mTOR and Akt signaling. Semin Immunol 2015:286–96. Elsevier.
[60] Wei Y, Liang M, Xiong L, Su N, Gao X, Jiang Z. PD-L1 induces macrophage polarization toward the M2 phenotype via Erk/Akt/mTOR. Experimental cell research 2021;402(2):112575.
[61] Won JE, Kim WJ, Shim JS, Ryu JJ. Guided bone regeneration with a nitric-oxide releasing polymer inducing angiogenesis and osteogenesis in critical-sized bone defects. Macromol Biosci 2022;22(10):2200162.